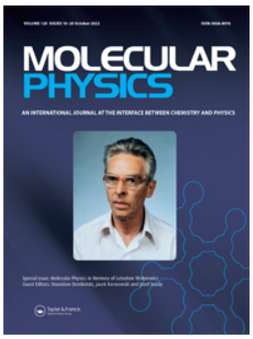

Taylor & Francis
Taylor & Francis Group

Molecular Physics

An International Journal at the Interface Between Chemistry and Physics

ISSN: (Print) (Online) Journal homepage: https://www.tandfonline.com/loi/tmph20

Analytic gradients for compressed multistate pair-density functional theory

Jie J. Bao, Matthew R. Hermes, Thais R. Scott, Andrew M. Sand, Roland Lindh, Laura Gagliardi & Donald G. Truhlar

To cite this article: Jie J. Bao, Matthew R. Hermes, Thais R. Scott, Andrew M. Sand, Roland Lindh, Laura Gagliardi & Donald G. Truhlar (2022) Analytic gradients for compressed multistate pair-density functional theory, Molecular Physics, 120:19-20, e2110534, DOI: 10.1080/00268976.2022.2110534

To link to this article: https://doi.org/10.1080/00268976.2022.2110534

MOLECULAR PHYSICS
2022, VOL. 120, NOS. 19–20, e2110534 (14 pages)
https://doi.org/10.1080/00268976.2022.2110534

Taylor & Francis
Taylor & Francis Group

L. WOLNIEWICZ SPECIAL ISSUE

Analytic gradients for compressed multistate pair-density functional theory

Jie J. Bao [a], Matthew R. Hermes [b,c], Thais R. Scott [b,c], Andrew M. Sand [d], Roland Lindh [e], Laura Gagliardi [b,c] and Donald G. Truhlar [a]

[a]Department of Chemistry, Chemical Theory Center, and Minnesota Supercomputing Institute, University of Minnesota, Minneapolis, MN, USA; [b]Department of Chemistry, Pritzker School of Molecular Engineering, James Franck Institute, Chicago Center for Theoretical Chemistry, The University of Chicago, Chicago, IL, USA; [c]Argonne National Laboratory, Lemont, IL, USA; [d]Department of Chemistry and Biochemistry, Butler University, Indianapolis, IN, USA; [e]Department of Chemistry–BMC, Uppsala University, Uppsala, Sweden

ABSTRACT

Photochemical reactions often involve states that are closely coupled due to near degeneracies, for example by proximity to conical intersections. Therefore, a multistate method is used to accurately describe these states; for example, ordinary perturbation theory is replaced by quasidegenerate perturbation theory. Multiconfiguration pair-density functional theory (MC-PDFT) provides an efficient way to approximate the full dynamical correlation energy of strongly correlated systems, and we recently proposed compressed multistate pair-density functional theory (CMS-PDFT) to treat closely coupled states. In the present paper, we report the implementation of analytic gradients for CMS-PDFT in both *OpenMolcas* and *PySCF*, and we illustrate the use of these gradients by applying the method to the excited states of formaldehyde and phenol.

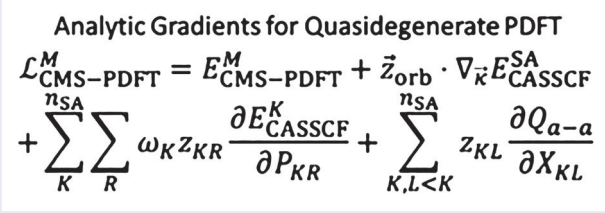

ARTICLE HISTORY
Received 16 February 2022
Accepted 21 July 2022

KEYWORDS
Analytic gradients; pair-density functional theory; electronic structure method; molecular geometry; excited states

1. Introduction

Photochemical reactions can involve highly multiconfigurational electronic states that have similar electronic energies [1]. Realistic dynamical simulations of photochemical reactions require accurate potential energy surfaces, and for such cases these can only be produced by a quantum-chemical model of electronic structure if that model is simultaneously able to represent (1) the static correlation of intrinsically multiconfigurational states that are not dominated by a single determinant, (2) the quantitative effect of dynamic electron correlation, and (3) state interaction, which requires the final approximations to the electronic states of interest to be simultaneous eigenvectors of the same matrix Hamiltonian. State interaction is responsible for topological features of adiabatic potential energy surfaces such as conical intersections and locally avoided crossings. Some examples of quantum-chemical electronic-structure methods that can model all three of these features are multireference configuration interaction (MRCI) [2,3], extended multiconfiguration quasi-degenerate perturbation theory (XMC-QDPT2) [4], quasi-degenerate *n*-electron valence perturbation theory (QD-NEVPT2) [5], extended multistate complete active space perturbation theory (XMS-CASPT2) [6], extended density-weighted CASPT2 (XDW-CASPT2) [7], and rotated multistate CASPT2 (RMS-CASPT2) [8]. In these methods, the step of the calculation responsible for modelling the full

CONTACT Roland Lindh roland.lindh@kemi.uu.se Department of Chemistry–BMC, Uppsala University, Uppsala 751 23, Sweden; Laura Gagliardi lgagliardi@uchicago.edu Department of Chemistry, Pritzker School of Molecular Engineering, James Franck Institute, Chicago Center for Theoretical Chemistry, The University of Chicago, Chicago, IL 60637, USA; Argonne National Laboratory, Lemont, IL 60439, USA; Donald G. Truhlar truhlar@umn.edu Department of Chemistry, Chemical Theory Center, and Minnesota Supercomputing Institute, University of Minnesota, Minneapolis, MN 55455, USA

We are pleased to contribute this manuscript to the special issue of *MolecularPhysics* honouring Lutosław Wolniewicz.

Supplemental data for this article can be accessed here. https://doi.org/10.1080/00268976.2022.2110534

dynamic electronic correlation (configuration interaction or perturbation theory) incurs significant computational cost.

Multiconfiguration pair-density functional theory (MC-PDFT) [9–11], in which the electronic energy is calculated by a functional of the kinetic energy, electron density, and on-top pair density of an underlying multiconfiguration wave function, provides an efficient alternative to those methods. The MC-PDFT method by itself defines an expression for the total energy of a state but does not provide a procedure for state interaction. We have proposed a state-interaction model and several multistate extensions to MC-PDFT to address this issue [12,13]. The multistate PDFT methods are more efficient, and they evaluate state interaction by rotating the basis of state-averaged complete-active-space self-consistent-field (SA-CASSCF) wave functions within a model space into an intermediate-state representation, such that the molecular Hamiltonian furnishes nonzero coupling elements between intermediate states, while their energies (diagonal elements of the model-space effective Hamiltonian) are evaluated using MC-PDFT. The most promising method appears to be what we have named compressed multistate PDFT (CMS-PDFT) [14]. The CMS-PDFT method defines the intermediate states as those linear combinations that maximise the sum of the classical Coulomb energies of the intermediate states, and this method was found to produce qualitatively correct and reasonably quantitatively accurate potential energy surfaces for a wide variety of systems exhibiting significant state interaction with a computational cost nearly equivalent to that of evaluating the same number of MC-PDFT total energies [14].

Here, we develop and implement analytic gradients of the CMS-PDFT state energies, which is an important step towards enabling practical *ab initio* nonadiabatic molecular dynamical simulations using this electronic structure method. The CMS-PDFT energy is not variational, and analytic gradients therefore require recasting CMS-PDFT energies in terms of a constrained energy minimisation for which the Lagrange multipliers must be evaluated [15,16], similar to cases treated previosuly for state-averaged CASSCF (SA-CASSCF) [17], MC-PDFT with a state-specific CASSCF reference wave function [18], MC-PDFT with a reference wave function from an SA-CASSCF calculation [19], and MC-PDFT with density fitting [20].

We implement the analytic gradients in two electronic structure programmes, and we numerically test our implementations by comparing them to one another and to numerical gradients. Furthermore, the structural parameters obtained by using the gradients to optimise the geometries of excited states and the excitation energies of the excited states are compared to those of other methods. In particular, properties are compared between the CMS-PDFT method and MC-PDFT calculations based on SA-CASSCF wave functions.

The rest of the paper is organised as follows: Section 2 briefly summarises the CMS-PDFT method for electronic energies and wave functions and presents the general algorithm and the structure of CMS-PDFT analytic gradient calculations; the Computational Details Section 3 presents the details of the computer simulations; the Results and Discussion Section 4 assesses the accuracy of the CMS-PDFT analytic gradients, the molecular structures, and the adiabatic excitation energies for selected molecules. Section 5 is a Conclusion Section. The article is supported with supplementary material containing additional programmable equations, optimised geometries, and gradient data.

2. Theory

Throughout this manuscript, lowercase letters other than *x*, *y*, *z* index molecular orbitals (MOs), and capital letters other than *X*, *Y*, *Z* index many-electron states within a given complete active space (CAS). Specific types of many-electron states are identified with specific letter ranges: *A*, *B* for configuration state functions (CSFs), including the special case of single determinants; *I*, *J* for SA-CASSCF reference states, *P*, *Q*, *R*, *S*, *T*, *U* for CMS-PDFT intermediate states, and *M*, *N* for CMS-PDFT final states. For MOs, *p*, *q*, *r*, *s*, *t* indicate general MOs, *i*, *j*, *k*, *l* indicate active MOs, *c* indicates an inactive (core) MO (which is doubly occupied in all configurations) and *a* indicates a virtual MO (which is unoccupied in all configurations).

The uppercase letters *X*, *Y*, *Z* indicate three different types of unitary group generators that define the wave function in the CMS-PDFT method: *X* for orbital rotations and *Y* and *Z* for many-electron state rotations (i.e. unitary transformations of the configuration interaction [CI] vectors). Rotations between two states that are both within a particular model space are indicated by *Z*, and rotations between a state within the model space and another state outside of it are indicated by *Y*. The lowercase letters *x*, *y*, *z* indicate a set of Lagrange multipliers for the corresponding uppercase-letter generators or their associated variables.

In what follows we proceed from the fundamentals of the CMS-PDFT energy to the details of constructing the corresponding nuclear gradients.

2.1. CMS-PDFT

CMS-PDFT energies and wave functions are the solutions to an eigenequation for an effective Hamiltonian

defined in a model space of $n_{SA} \geq 2$ multideterminantal wave functions:

$$|N\rangle \langle N|\hat{H}^{CMS}|M\rangle = |N\rangle \delta_{MN} E_M^{CMS}, \quad (1)$$

where

$$\hat{H}^{CMS} = \sum_{P\neq Q}^{n_{SA}} |P\rangle H_{PQ} \langle Q| + \sum_{P}^{n_{SA}} |P\rangle E_P^{PDFT} \langle P|, \quad (2)$$

where $H_{PQ} \equiv \langle P|\hat{H}|Q\rangle$ is a matrix element of the molecular electronic Hamiltonian and

$$E_P^{PDFT} = V_{NN} + \sum_{p,q} h_{pq} D_{pq}^{PP} + \frac{1}{2} \sum_{p,q,r,s} g_{pqrs} D_{pq}^{PP} D_{rs}^{PP} + E_{OT}[\rho_P, \Pi_P], \quad (3)$$

is the MC-PDFT energy expression: V_{NN} for the internuclear Coulomb repulsion; h and g respectively for the one- and two-electron Hamiltonian interaction elements; D^{PP}, ρ_P, and Π_P respectively for the one-body reduced density matrix (1-RDM), density, and on-top pair density for state P; and $E_{OT}[\rho_P, \Pi_P]$ for the on-top energy functional that provides the energetic contributions due to electron correlation and exchange.

The states $|P\rangle$, $|Q\rangle$, etc. defining $\hat{H}^{CMS}$ in Equation (2) span a model space constructed by an underlying SA-CASSCF calculation,

$$|P\rangle = \sum_I |I\rangle \langle I|P\rangle, \quad (4)$$

where $|I\rangle$ are SA-CASSCF wave functions. The unitary transformation coefficients ($\langle I|P\rangle$) are determined by maximising the sum of the classical electron-electron Coulomb energies under rotation of the states defining the model space,

$$\langle I|P\rangle = \text{argmax} Q_{a-a}, \quad (5)$$

$$Q_{a-a} \equiv \frac{1}{2} \sum_P \sum_{i,j,k,l} g_{ijkl} D_{ij}^{PP} D_{kl}^{PP}. \quad (6)$$

The transformation from the SA-CASSCF basis ($|I\rangle, |J\rangle$) to the CMS-PDFT intermediate-state basis ($|P\rangle, |Q\rangle$) is necessary because PDFT does not furnish a way to approximate the Hamiltonian matrix elements coupling different states. Furthermore, in the SA-CASSCF basis, the off-diagonal Hamiltonian matrix elements appearing in Equation (2) are identically zero by construction and therefore cannot be used to treat state interaction. The motivation for the specific form of the objective function defining the intermediate states, Q_{a-a} in Equation (6), is described in Ref. [14].

2.2. Derivatives of the CMS objective function

In anticipation of the requirements of Section 2.3 below, we here present the first and second derivatives of the CMS-PDFT objective function, Q_{a-a}, with respect to rotation between intermediate states. These derivatives can be utilised in a straightforward way to implement a Newton-Raphson gradient-descent algorithm for solving Equation (5) above, although this was not the algorithm implemented originally in the previous work presenting the CMS-PDFT method [14].

Parameterising intermediate state $|P\rangle$ as

$$|P\rangle \rightarrow \exp\left[\hat{Z}\right] |P\rangle, \quad (7)$$

with

$$\hat{Z} = \sum_{P>Q} Z_{PQ} \left(|Q\rangle \langle P| - |P\rangle \langle Q|\right), \quad (8)$$

and defining

$$W_{QS}^{PR} \equiv \sum_{i,j,k,l} g_{ijkl} D_{ij}^{PQ} D_{kl}^{RS}, \quad (9)$$

$$V_{QS}^{PR} \equiv \delta_{QR} \left(W_{SS}^{PS} + W_{PP}^{SP} - W_{SQ}^{PQ} - W_{SR}^{PR} - 4W_{QS}^{PR}\right), \quad (10)$$

where D^{PQ} is the one-body transition density matrix between states P and Q, we have

$$Q_{a-a} = \frac{1}{2} \sum_P W_{PP}^{PP}, \quad (11)$$

$$\frac{\partial Q_{a-a}}{\partial Z_{PQ}} = 2\left(W_{PP}^{QP} - W_{QQ}^{PQ}\right), \quad (12)$$

$$\frac{\partial^2 Q_{a-a}}{\partial Z_{PQ} \partial Z_{RS}} = V_{QS}^{PR} - V_{PS}^{QR} - V_{QR}^{PS} + V_{PR}^{QS}. \quad (13)$$

The solution of Equation (5) corresponds to a stationary point at which the Hessian is negative-definite,

$$\frac{\partial Q_{a-a}}{\partial Z_{PQ}} = 0, \quad (14)$$

$$\mathbf{H}_{ZZ}^{Q_{a-a}} \prec 0, \quad (15)$$

where $\mathbf{H}_{ZZ}^{Q_{a-a}}$ is the Hessian matrix with elements given by Equation (13).

2.3. Analytic gradient formalism

It is straightforward to demonstrate that the final CMS-PDFT energies, E_M^{CMS}, are stationary with respect to their expansion coefficients in terms of the intermediate states, $\langle P|M\rangle$. Therefore, the derivatives of the expansion

coefficients upon perturbation of the physical Hamiltonian do not contribute to the molecular gradients of the CMS-PDFT energies. As a consequence, differentiation of CMS-PDFT effective Hamiltonian matrix elements can be substituted for differentiation of CMS-PDFT final state total energies without loss of generality,

$$\mathrm{d}E_M^{\mathrm{CMS}} = \sum_{P,Q} \langle M|P\rangle \, \mathrm{d}H_{PQ}^{\mathrm{CMS}} \, \langle Q|M\rangle \,, \tag{16}$$

which is convenient because partial derivatives of H_{PQ}^{CMS} have simpler programmable expressions than those of E_M^{CMS} due to the form of Equation (2). Therefore, in the following, we will consider the gradient of H_{PQ}^{CMS} rather than that of E_M^{CMS} directly, with the understanding that the unitary transformation described by Equation (16) is applied to any equation in which $\partial H_{PQ}^{\mathrm{CMS}}$ or dH_{PQ}^{CMS} appears.

The matrix elements of the effective Hamiltonian are not stationary with respect to their orbital coefficients and CI vectors. Therefore, the Hellmann-Feynman theorem does not apply, and we instead make use of Lagrange's method of undetermined multipliers to recast the expressions for H_{PQ}^{CMS} as the solutions to a constrained-optimisation problem. We parameterise the intermediate-state wave functions as

$$|P\rangle \rightarrow \exp\left[\hat{X}\right] \exp\left[\hat{Y}\right] \exp\left[\hat{Z}\right] |P\rangle \,, \tag{17}$$

where $\hat{Z}$ is defined by Equation (8) and

$$\hat{X} = \sum_{p>q} \sum_{\sigma} X_{pq} \left(\hat{c}_{p\sigma}^{\dagger} \hat{c}_{q\sigma} - \hat{c}_{q\sigma}^{\dagger} \hat{c}_{p\sigma} \right), \tag{18}$$

$$\hat{Y} = \sum_{P,A} Y_{PA} \left(\hat{Q}_{\mathrm{SA}} \, |A\rangle \, \langle P| - |P\rangle \, \langle A| \, \hat{Q}_{\mathrm{SA}} \right), \tag{19}$$

where $\hat{c}_{p\sigma}^{\dagger}$ ($\hat{c}_{p\sigma}$) creates (annihilates) an electron of spin σ in the pth orbital, where $|A\rangle$ is a single determinant or CSF, and where

$$\hat{Q}_{\mathrm{SA}} \equiv 1 - \sum_{P} |P\rangle \, \langle P| \,. \tag{20}$$

The variables X_{pq} and Y_{PA}, respectively, denote rotations between orbitals and rotations between many-electron states within the model space and those outside of it. The latter need to be explicitly separated from the rotations between two states within the model space [Z_{PQ} from Equation (8)] using the projection operator $\hat{Q}_{\mathrm{SA}}$, because Y_{PA} and Z_{PQ} satisfy two unrelated sets of optimisation conditions in the CMS-PDFT energy calculation. The effect of the projection operator is accounted for by requiring that every row of the matrix Y (and its corresponding Lagrange-multiplier matrix y; see below) is orthogonal to all intermediate states (or equivalently to all reference or final states):

$$\sum_{A} Y_{PA} \, \langle A|Q\rangle = 0 \quad \forall \, P, Q. \tag{21}$$

The minimisation of the state-averaged energy of the underlying SA-CASSCF calculation (E_{CAS}) determines X and Y, whereas Equations (14) and (15) determines Z, so the Lagrangian for CMS-PDFT is written as

$$\mathcal{L}_{PQ}^{\mathrm{CMS}} = H_{PQ}^{\mathrm{CMS}} + \sum_{p>q} \frac{\partial E_{\mathrm{CAS}}}{\partial X_{pq}} x_{pq} + \sum_{R,A} \frac{\partial E_{\mathrm{CAS}}}{\partial Y_{RA}} y_{RA} + \sum_{R>S} \frac{\partial Q_{\mathrm{a-a}}}{\partial Z_{RS}} z_{RS}, \tag{22}$$

where, as a reminder, uppercase X, Y, Z indicate the wave function variables and lowercase x, y, z indicate the corresponding Lagrange multipliers. The values of the latter are determined by solving for

$$\frac{\partial \mathcal{L}_{PQ}^{\mathrm{CMS}}}{\partial X_{pq}} = \frac{\partial \mathcal{L}_{PQ}^{\mathrm{CMS}}}{\partial Y_{RA}} = \frac{\partial \mathcal{L}_{PQ}^{\mathrm{CMS}}}{\partial Z_{RS}} = 0, \tag{23}$$

so that the Lagrangian is stationary in X, Y, Z, x, y, and z. The dependence of these parameters on the molecular geometry can therefore be neglected when evaluating the molecular gradient,

$$\frac{\mathrm{d}H_{PQ}^{\mathrm{CMS}}}{\mathrm{d}\lambda} = \frac{\mathrm{d}\mathcal{L}_{PQ}^{\mathrm{CMS}}}{\mathrm{d}\lambda} = \frac{\partial \mathcal{L}_{PQ}^{\mathrm{CMS}}}{\partial \lambda}. \tag{24}$$

2.4. Determination of the Lagrange multipliers

Substituting Equation (22) into (23) yields a system of coupled linear equations,

$$\begin{pmatrix} \nabla_X H_{PQ}^{\mathrm{CMS}} \\ \nabla_Y H_{PQ}^{\mathrm{CMS}} \\ \nabla_Z H_{PQ}^{\mathrm{CMS}} \end{pmatrix} + \begin{pmatrix} \mathbf{H}_{XX}^{E_{\mathrm{CAS}}} & \mathbf{H}_{XY}^{E_{\mathrm{CAS}}} & \mathbf{H}_{XZ}^{Q_{\mathrm{a-a}}} \\ \mathbf{H}_{YX}^{E_{\mathrm{CAS}}} & \mathbf{H}_{YY}^{E_{\mathrm{CAS}}} & \mathbf{H}_{YZ}^{Q_{\mathrm{a-a}}} \\ 0 & 0 & \mathbf{H}_{ZZ}^{Q_{\mathrm{a-a}}} \end{pmatrix} \begin{pmatrix} \vec{x} \\ \vec{y} \\ \vec{z} \end{pmatrix} = \begin{pmatrix} 0 \\ 0 \\ 0 \end{pmatrix}, \tag{25}$$

where $\vec{x}, \ldots, \nabla_X, \ldots$, and $\mathbf{H}_{XX}^{f}, \ldots$ are vectors of Lagrange multipliers, vectors of first derivatives with respect to wave function variables, and Hessian matrix blocks of some function f with respect to wave function variables, respectively.

Some of the elements of the second-derivative matrix in Equation (25) are zero by construction, because E_{CAS} is insensitive to rotations among intermediate states. The sole nonzero block in the Z rows, $\mathbf{H}_{ZZ}^{Q_{\mathrm{a-a}}}$, was presented in

Section 2.2, and we assume that the model space is small enough to store it in memory and invert it noniteratively,

$$\vec{z} = -\left(\mathbf{H}_{ZZ}^{\mathrm{Q_{a-a}}}\right)^{-1} \cdot \nabla_Z H_{PQ}^{\mathrm{CMS}}. \tag{26}$$

We then solve for $\vec{x}$ and $\vec{y}$ with $\vec{z}$ fixed by rearranging Equation (25):

$$\begin{pmatrix} \nabla_X H_{PQ}^{\mathrm{CMS}} + \mathbf{H}_{XZ}^{\mathrm{Q_{a-a}}} \cdot \vec{z} \\ \nabla_Y H_{PQ}^{\mathrm{CMS}} + \mathbf{H}_{YZ}^{\mathrm{Q_{a-a}}} \cdot \vec{z} \end{pmatrix} + \begin{pmatrix} \mathbf{H}_{XX}^{E_{\mathrm{CAS}}} & \mathbf{H}_{XY}^{E_{\mathrm{CAS}}} \\ \mathbf{H}_{YX}^{E_{\mathrm{CAS}}} & \mathbf{H}_{YY}^{E_{\mathrm{CAS}}} \end{pmatrix} \begin{pmatrix} \vec{x} \\ \vec{y} \end{pmatrix} = \begin{pmatrix} 0 \\ 0 \end{pmatrix}, \tag{27}$$

using the standard preconditioned conjugate gradient iterative solver.

Most of the gradient vectors and Hessian blocks appearing in Equations (25)–(27) are slight modifications or straightfoward generalisations of similar quantities that appear in the programmable equations for SA-CASSCF [17] or MC-PDFT based on SA-CASSCF wave functions [19]. For instance, the Hessian of the SA-CASSCF average energy, $\mathbf{H}^{E_{\mathrm{CAS}}}$, is well-established and is unchanged in the context of CMS-PDFT inasmuch as the Y sectors are expressed in the reference-state basis ($|I\rangle, |J\rangle$). (In practice, we evaluate the Hessian-vector product of $\mathbf{H}_{YY}^{E_{\mathrm{CAS}}}$ in the intermediate-state basis ($|P\rangle, |Q\rangle$); this modifies the form of the equation somewhat, as described in Section 1 of the supplementary material.)

The driving vector of Equation (25) ($\nabla_X, \nabla_Y, \nabla_Z$) is either a minor generalisation of the energy response for MC-PDFT with an SA-CASSCF wave function [19], or an off-diagonal generalisation of the SA-CASSCF energy response [17], depending on the indices P and Q:

$$\left\{\nabla_X H_{PQ}^{\mathrm{CMS}}\right\}_{pq} = \begin{cases} \frac{\partial E_P^{\mathrm{PDFT}}}{\partial X_{pq}} & P = Q \\ \frac{\partial H_{PQ}}{\partial X_{pq}} & \text{otherwise} \end{cases}, \tag{28}$$

$$\left\{\nabla_Y H_{PQ}^{\mathrm{CMS}}\right\}_{RA} = \begin{cases} \frac{\partial E_P^{\mathrm{PDFT}}}{\partial Y_{RA}} & P = Q \\ \frac{\partial H_{PQ}}{\partial Y_{RA}} & \text{otherwise} \end{cases}, \tag{29}$$

$$\left\{\nabla_Z H^{\mathrm{CMS}}{}_{PQ}\right\}_{RS} = \begin{cases} \frac{\partial E_P^{\mathrm{PDFT}}}{\partial Z_{RS}} & P = Q \\ \frac{\partial H_{PQ}}{\partial Z_{RS}} & \text{otherwise} \end{cases}. \tag{30}$$

In the diagonal case, we define

$$\hat{A} = \sum_{P,A} A_{PA} \left(|A\rangle \langle P| - |P\rangle \langle A|\right), \tag{31}$$

[i.e. $\hat{Y}$ from Equation (19) without the projection operator, $\hat{Q}_{\mathrm{SA}}$], and evaluate

$$\frac{\partial E_P^{\mathrm{PDFT}}}{\partial X_{pq}}, \quad \frac{\partial E_P^{\mathrm{PDFT}}}{\partial A_{PA}} \tag{32}$$

via Equations (28) and (29), respectively, of Ref. [19], using the intermediate-state CI vectors, densities, and density matrices of $|P\rangle$ rather than the SA-CASSCF reference-state quantities. The Y and Z components of the latter are then separated,

$$\frac{\partial E_P^{\mathrm{PDFT}}}{\partial Z_{RS}} = \delta_{RP} \sum_A \frac{\partial E_P^{\mathrm{PDFT}}}{\partial A_{PA}} \langle A|S\rangle - \delta_{SP} \sum_A \frac{\partial E_P^{\mathrm{PDFT}}}{\partial A_{PA}} \langle A|R\rangle, \tag{33}$$

$$\frac{\partial E_P^{\mathrm{PDFT}}}{\partial Y_{RA}} = \delta_{RP} \left(\frac{\partial E_P^{\mathrm{PDFT}}}{\partial A_{PA}} - \sum_{S<P} \frac{\partial E_P^{\mathrm{PDFT}}}{\partial Z_{PS}} \langle A|S\rangle + \sum_{S>P} \frac{\partial E_P^{\mathrm{PDFT}}}{\partial Z_{SP}} \langle A|S\rangle \right), \tag{34}$$

It is important to remember that Z_{RS} is only defined for $R > S$.

In the off-diagonal case of Equations (28)–(30), we have

$$\frac{\partial H_{PQ}}{\partial X_{pq}} = F_{pq}^{PQ} - F_{qp}^{PQ} + F_{pq}^{QP} - F_{qp}^{QP}, \tag{35}$$

$$\frac{\partial H_{PQ}}{\partial Y_{RA}} = 0, \tag{36}$$

$$\frac{\partial H_{PQ}}{\partial Z_{RS}} = \delta_{QR} H_{PS} - \delta_{QS} H_{PR} + \delta_{PR} H_{SQ} - \delta_{PS} H_{RQ} \tag{37}$$

with

$$F_{pq}^{PQ} \equiv \sum_r h_{pr} D_{qr}^{PQ} + \sum_{r,s,t} g_{prst} d_{qrst}^{PQ}, \tag{38}$$

where d^{PQ} is the two-body transition density matrix.

What remains are only the off-diagonal Hessian-vector products of the CMS-PDFT intermediate-state objective function, $\mathbf{H}^{\mathrm{Q_{a-a}}}$, appearing in the first term on the left-hand side of Equation (27). In order to express these terms concisely, we introduce additional Coulomb-potential intermediates related to W_{QS}^{PR} defined in Equation (9) above,

$$\hat{W}_Q^P = \sum_{i,j,k,l} g_{ijkl} D_{kl}^{PQ} \sum_\sigma \hat{c}_{i\sigma}^\dagger \hat{c}_{j\sigma}, \tag{39}$$

so that $W_{QS}^{PR} = \langle R|\hat{W}_Q^P|S\rangle = \langle P|\hat{W}_S^R|Q\rangle$. We also introduce effective density matrices and CMS generalised

Fock matrices,

$$\tilde{D}^{PP}_{ij} \equiv \sum_{Q} \left(D^{PQ}_{ij} + D^{QP}_{ij} \right) \tilde{z}_{PQ}, \tag{40}$$

$$F^{Q_{a-a}}_{pi} \equiv \sum_{j,k,l} g_{pjkl} \sum_{P} \left(\tilde{D}^{PP}_{ij} D^{PP}_{kl} + D^{PP}_{ij} \tilde{D}^{PP}_{kl} \right), \tag{41}$$

$$F^{Q_{a-a}}_{pc} = F^{Q_{a-a}}_{pa} = 0, \tag{42}$$

where $\tilde{z}_{PQ}$ is

$$\tilde{z}_{PQ} = \begin{cases} z_{PQ} & P > Q \\ -z_{QP} & Q > P \end{cases}. \tag{43}$$

Using these intermediates, the Hessian-vector products in the first term on the left-hand side of Equation (27) have the elements

$$\left\{ \mathbf{H}^{Q_{a-a}}_{XZ} \cdot \vec{z} \right\}_{pq} \equiv \sum_{P>Q} \frac{\partial^2 Q_{a-a}}{\partial X_{pq} \partial Z_{PQ}} z_{PQ} = 2 \left(F^{Q_{a-a}}_{pq} - F^{Q_{a-a}}_{qp} \right), \tag{44}$$

$$\left\{ \mathbf{H}^{Q_{a-a}}_{YZ} \cdot \vec{z} \right\}_{PA} \equiv \sum_{Q>R} \frac{\partial^2 Q_{a-a}}{\partial Y_{PA} \partial Z_{QR}} z_{QR} = \langle A | \hat{Q}_{SA} \sum_{Q} \tilde{z}_{PQ} \times \left(4 \hat{W}^{P}_{Q} | P \rangle + 2 \left(\hat{W}^{P}_{P} - \hat{W}^{Q}_{Q} \right) | Q \rangle \right). \tag{45}$$

2.5. Nuclear-coordinate derivatives of the Lagrangian

Having determined the Lagrange multipliers by solving Equation (23), it remains to evaluate the molecular gradient by differentiating the Lagrangian itself [Equation (24)]:

$$\frac{\partial \mathcal{L}^{CMS}_{PQ}}{\partial \lambda} = \frac{\partial H^{CMS}_{PQ}}{\partial \lambda} + \sum_{p>q} \frac{\partial^2 E_{CAS}}{\partial \lambda \partial X_{pq}} x_{pq} + \sum_{R,A} \frac{\partial^2 E_{CAS}}{\partial \lambda \partial Y_{RA}} y_{RA} + \sum_{R>S} \frac{\partial^2 Q_{a-a}}{\partial \lambda \partial Z_{RS}} z_{RS}. \tag{46}$$

The first-term on the right-hand side of Equation (46) is the Hellmann-Feynman term and, just like the driving vector above, it differs depending on whether one is considering a diagonal or off-diagonal element:

$$\frac{\partial H^{CMS}_{PQ}}{\partial \lambda} = \begin{cases} \frac{\partial E^{PDFT}_{P}}{\partial \lambda} & P = Q \\ \frac{\partial H_{PQ}}{\partial \lambda} & \text{otherwise} \end{cases}. \tag{47}$$

In the diagonal case, the Hellmann-Feynman contribution is essentially the same as in MC-PDFT based on an SA-CASSCF wave function [19], except that intermediate state $|P\rangle$ is used instead of a SA-CASSCF reference state:

$$\frac{\partial E^{PDFT}_{P}}{\partial \lambda} = \frac{\partial V_{NN}}{\partial \lambda} + \sum_{p,q} \frac{\partial h_{pq}}{\partial \lambda} D^{PP}_{pq} + \frac{1}{2} \sum_{p,q,r,s} \frac{\partial g_{pqrs}}{\partial \lambda} D^{PP}_{pq} D^{PP}_{rs} + \frac{\partial E_{OT}[\rho_P, \Pi_P]}{\partial \lambda} - \sum_{p,q} \frac{\partial s_{pq}}{\partial \lambda} F^{(OT)}_{pq}, \tag{48}$$

where s_{pq} is the overlap matrix between MOs p and q, the derivatives are partial because the MO coefficients are treated as fixed, and $\partial E_{OT}[\rho_P, \Pi_P]/\partial \lambda$ and $F^{(OT)}_{pq}$ are given by Equations (49) and (31) of Ref. [19], respectively. In the off-diagonal case, the Hellmann-Feynman contribution is like that of SA-CASSCF [17], except that transition density matrices coupling $|P\rangle$ and $|Q\rangle$ are used instead of the reduced density matrices of SA-CASSCF reference states and the internuclear potential term is omitted:

$$\frac{\partial H_{PQ}}{\partial \lambda} = \sum_{p,q} \frac{\partial h_{pq}}{\partial \lambda} D^{PQ}_{pq} + \frac{1}{2} \sum_{p,q,r,s} \frac{\partial g_{pqrs}}{\partial \lambda} d^{PQ}_{pqrs} - \frac{1}{2} \sum_{p,q} \frac{\partial s_{pq}}{\partial \lambda} \left(F^{PQ}_{pq} + F^{QP}_{pq} \right). \tag{49}$$

The second and third terms on the right-hand side of Equation (46) are also equivalent to corresponding terms in both SA-CASSCF [17] and MC-PDFT based on SA-CASSCF [19], except that CMS-PDFT intermediate-state quantities are used instead of SA-CASSCF reference-state quantities. The fourth term is unique to CMS-PDFT:

$$\sum_{P>Q} \frac{\partial^2 Q_{a-a}}{\partial \lambda \partial Z_{PQ}} z_{PQ} = \sum_{p,q,r,s} \frac{\partial g_{pqrs}}{\partial \lambda} \sum_{P} \left(D^{PP}_{pq} \tilde{D}^{PP}_{rs} \right) - \sum_{p,q} \frac{\partial s_{pq}}{\partial \lambda} F^{Q_{a-a}}_{pq}. \tag{50}$$

2.6. A note about undefined gradients

During numerical tests, we discovered cases in which the gradient of CMS-PDFT potential energy surfaces were undefined. For example, Q_{a-a} is invariant to rotations between degenerate Π states of linear molecules, rendering the optimised intermediate-state basis arbitrary; but the corresponding PDFT state energies (which depend in practice on a finite quadrature grid) are generally noninvariant to this rotation, rendering the CMS-PDFT final energies non-unique. (N.B.: the test calculations of diatomic molecular gradients presented

in Sections 3 and 4 below include only Σ states in the model space.) We find that the behaviour of our implementations is reliably controlled in these cases by setting to zero any z_{RS} Lagrange multiplier whose magnitude after evaluation of Equation (26) is unphysically large. The wave function is periodic in the corresponding unitary generator amplitudes (Z_{RS}), and for a two-state model space, the period is 2π. We therefore use a magnitude of 2π as our threshold past which z_{RS} is set to zero. If the corresponding element of $\nabla_Z H_{PQ}^{\mathrm{CMS}}$ is sufficiently small, such that Equation (25) can be solved to within a satisfactory threshold despite setting $z_{RS} = 0$ by *fiat*, then the Lagrange multiplier was redundant and is safely omitted. Otherwise, the specified CMS-PDFT gradient is implied to be undefined at the specified geometry.

3. Computational procedure

The gradient calculations are performed in both *OpenMolcas* version 22.06, commit SHA-1 f45278022 [21,22], and *mrh* [23] (commit SHA-1 92f7542b4), an extension of *PySCF* [24] version 2.0.1 (commit SHA-1 f985dde73). In the latter implementation, the plugin for *geomeTRIC* [25] version 0.9.7.2 was used to optimise geometries. In *OpenMolcas* calculations, the 'ultrafine' numerical quadrature grid (99 radial shells and 590 angular points for each atom, and a crowding factor of 10 and a fade factor of 10 for pruning angular grids) is used, and the rotational invariance of the quadrature grid is deactivated using the 'NORO' keyword. In *PySCF*, the quadrature grid was set to level 6 (80/120 radial and 770/974 angular for atoms of period 1/2 respectively). For numerical gradient calculations in *OpenMolcas*, a locally modified version based on the commit SHA-1 de7464102 is used so that 11 significant figures are printed for numerical gradients. We tested our gradient code on three diatomics, namely HeH^+, LiH and LiF, and two polyatomics, namely HCHO and phenol. The reason for testing the analytic gradient code on diatomic molecules is that the results can be easily compared with numerical ones. The procedure of each calculation is listed in Table 1.

Table 1. Number of states in the model space n_{SA}, active space, (n_e, n_o), basis set, functional and the programme used in the gradient calculations for each molecule.

Molecule	n_{SA}	Active Space	Basis Set	Functional	Programme
HeH^+	2	(2, 2)	cc-pVDZ [26]	ftLSDA	*OpenMolcas* *PySCF*
LiH	2	(2, 2)	aug-cc-pVTZ [26]	tPBE	*OpenMolcas*
LiF	2	(8, 5)	jun-cc-pVTZ [27]	tPBE	*OpenMolcas*
HCHO	2	(6, 5)	jun-cc-pVTZ	tPBE	*OpenMolcas*
phenol	3	(12, 11)	jul-cc-pVDZ [27]	tPBE	*PySCF*

4. Results and discussion

We confirm the correctness of the analytic gradients, and we compare them to numerically derived values for a small set of molecules. After that, we consider the validity and accuracy of the CMS-PDFT method for the evaluation of molecular structure parameters and vertical and adiabatic excitation energies for the formaldehyde and phenol molecules by comparison to results obtained by other high-quality methods.

4.1. Diatomic molecules

We probe the agreement between analytic and numerical CMS-PDFT gradient calculations using the potential energy curves of the diatomic molecules HeH^+ [28–32], LiH [33–37], and LiF [38–40]. The gradients for the diatomic systems can be obtained numerically in a straightforward way, so testing the analytic gradients against the numerical gradients for these diatomic systems is a convenient way to verify that the gradient codes give correct answers.

Because the calculated numerical gradient depends on the geometry displacement (Δ) used in the calculation, the most accurate way for obtaining a gradient accurately is to run the numerical gradient calculations for various geometrical displacements, and extrapolate the results to the $\Delta = 0$ limit. We use the linear regression of the numerical gradient versus Δ^2 for a subset of data with a coefficient of determination R^2 greater than 0.9 (most of them are greater than 0.999), and we take the intercept as the numerical gradient extrapolated to the $\Delta = 0$ limit. The numerical gradients that do not have a strong linear dependence on Δ^2 ($R^2 < 0.9$) are discarded (The only data point that is discarded is the one for the second state of LiH at 2.6 Å.). This extrapolation is undertaken because the magnitudes of these gradients, as well as the corresponding curvatures, span many orders of magnitude, due to the strongly bound character of the electronic ground states of these molecules. We note that there are numerical errors in both numerical and analytic gradients, because both are obtained from a wave function whose energy is converged to a finite digit after the decimal place (10^{-8} hartree). Therefore, the unbiased interpretation of comparing the numerical and analytic gradients is that, if two gradients disagree by a big number (e.g. 0.1 hartree/bohr), it means that at least one gradient is wrong. But when two gradients agree, it is more likely that both gradients are computed correctly to the digit where they agree. However, for the convenience of the discussion and following the convention we used before [20], in the rest of the paper, we set the numerical gradients as the reference.

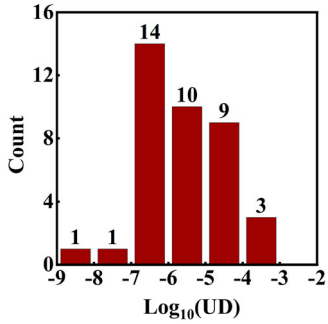

Figure 1. The distribution of the common logarithm of the unsigned difference, $\log_{10}(\mathrm{UD})$, in analytic gradients for HeH^+.

Additionally, we compare the analytic gradient for HeH^+ computed with the two separate implementations (*OpenMolcas* and *PySCF*-based). (HeH^+ with a double-ζ basis set, a (2, 2) active space, and 2 states in the model space is essentially the smallest possible testbed in which all four terms on the right-hand side of Equation (46) make a non-vanishing contribution to the gradient.)

The accuracy of the analytic gradients is evaluated by two quantities, namely the common logarithm of the unsigned error, $\log_{10}(\mathrm{UE})$, and the common logarithm of the relative unsigned error, $\log_{10}(\mathrm{RE})$.

$$\log_{10}(\mathrm{UE}) = \log_{10}(|\mathrm{Ana} - \mathrm{Num}|) \quad (51)$$

$$\log_{10}(\mathrm{RE}) = \log_{10}(|\mathrm{Ana} - \mathrm{Num}|/|\mathrm{Num}|) \quad (52)$$

where 'Ana' and 'Num' are the analytic and the numerical gradients, respectively, and the unit for the gradient is hartree/bohr. The common logarithm of the unsigned difference (UD) is used to determine whether the analytic gradients obtained with the two codes agree with each other.

$$\log_{10}(\mathrm{UD}) = \log_{10}(|\mathrm{Ana}_{OpenMolcas} - \mathrm{Ana}_{PySCF}|) \quad (53)$$

where $\mathrm{Ana}_{OpenMolcas}$ and Ana_{PySCF} are the analytic gradients for two programmes, respectively.

We observe that these errors and differences show little consistent correlation to the internuclear separation when extrapolating to the $\Delta = 0$ limit (cf. Section 2 of the supplementary information). However, in all cases, their magnitudes occur in a roughly normal distribution, and therefore we present this data in the form of histograms in Figures 1–4 below.

The distribution of $\log_{10}(\mathrm{UD})$ between two programmes is shown in Figure 1. In Figure 1, most of the differences in the analytic gradients are less than 10^{-4} hartree/bohr, and the greatest difference is 2.3×10^{-4} hartree/bohr at 0.4 Å for the ground state, where the gradient at this geometry is 1.6 hartree/bohr, meaning that the relative deviation between the two codes is about

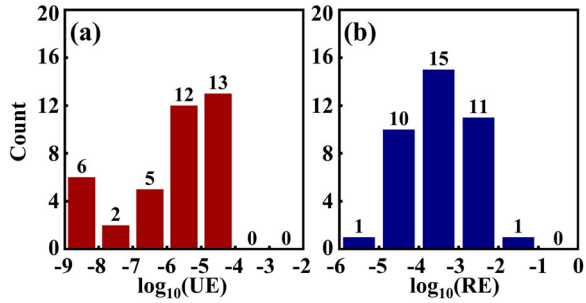

Figure 2. The distribution for the common logarithms of the unsigned error, $\log_{10}(\mathrm{UE})$, and the relative unsigned error, $\log_{10}(\mathrm{RE})$, for the analytic gradients for HeH^+ calculated in *OpenMolcas*.

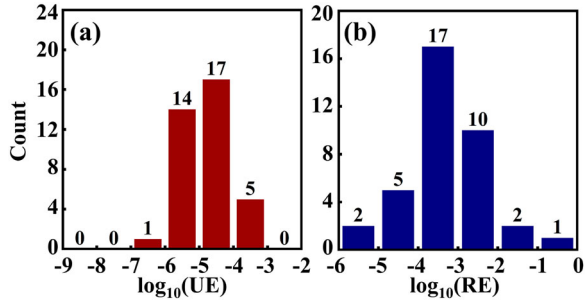

Figure 3. The distribution for the common logarithms of the unsigned error, $\log_{10}(\mathrm{UE})$, and the relative unsigned error, $\log_{10}(\mathrm{RE})$, for the analytic gradients for LiH calculated in *OpenMolcas*.

1.4×10^{-4}. We therefore conclude that the analytic gradients from one code agree very well with those from the other.

In Figures 2–4, we show the distribution of the $\log_{10}(\mathrm{UE})$ and $\log_{10}(\mathrm{RE})$ for HeH^+, LiH and LiF. We also show the $\log_{10}(\mathrm{UE})$ and $\log_{10}(\mathrm{RE})$ of these systems in Figures S1–S3 in Section S2 in the supplementary material. We see from Figures 2 to 4 that the unsigned errors in most cases are below 10^{-4} hartree/bohr. There are a few exceptions for LiH and LiF. These relatively larger errors are coming from the difficulties in getting very accurate numerical gradients because the data used for fitting come from relatively discrete Δ values. The relative unsigned errors are in most cases less than 1% for the three systems. The outlier values are either in the dissociated region for HeH^+, or at the equilibrium distance (1.6 Å) for LiH. Note that the gradients are small in both dissociation and equilibrium regions.

The statistics of the analytic gradients are shown in Table 2. We see that the analytic gradients systematically underestimate the numerical gradients by about 10^{-5} to 10^{-6} hartree/bohr, and the root-mean-squared error (RMSE) is about 10^{-5} hartree/bohr. The statistics

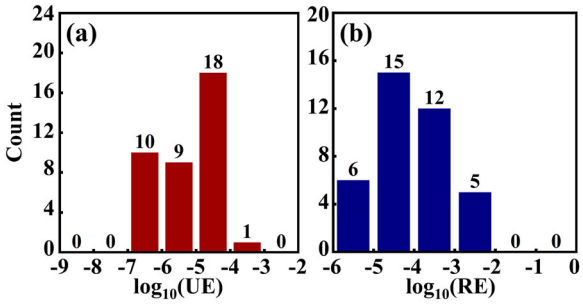

Figure 4. The distribution for the common logarithms of the unsigned error, $\log_{10}$(UE), and the relative unsigned error, $\log_{10}$(RE), for the analytic gradients for LiF calculated in *OpenMolcas*.

Table 2. The mean signed error (MSE), mean unsigned error (MUE) and root-mean-squared error (RMSE) of the analytic gradients estimated as deviations from the numerical gradients for HeH^+, LiH, LiF, and all three systems combined (units: hartree/bohr).

	HeH^+	LiH	LiF	All
MSE	7.0E−06	−7.6E−06	−2.2E−06	−4.1E−06
MUE	1.4E−05	4.9E−05	2.1E−05	2.8E−05
RMSE	2.4E−05	1.3E−04	4.7E−05	8.2E−04

in Table 2 show that the accuracy and the uncertainty of the CMS-PDFT numerical gradients are both about 10^{-5} hartree/bohr. This is consistent with our previous observed for the MC-PDFT gradients [20], where it states 'The mean unsigned deviation (MUD) for the SA-PDFT analytic gradients compared to the numerical gradients is 4×10^{-5} hartree bohrs^{-1}'.

In addition to comparing analytic and numeric gradients, we have performed a geometry optimisation for LiH. In Table 3, we tabulate the equilibrium distances for the first two states of LiH. We found that CMS-PDFT performs as well as MC-PDFT for predicting the ground state equilibrium distance. Although CMS-PDFT gives a good ground-state geometry, it does not give an accurate equilibrium distance for the first excited state. We note that predicting the equilibrium distance of the first excited state of LiH is an especially difficult problem because the potential curve of this state is abnormally flat in the vicinity of its minimum [36]. Therefore, we conclude that CMS-PDFT gives a reasonably good geometry for the first excited state of LiH.

4.2. Formaldehyde

Formaldehyde is planar and has C_{2v} symmetry in the ground state. In the first excited state, formaldehyde is nonplanar, and the angle between the C=O bond and the H–C–H plane, denoted as η, is used to describe the nonplanarity.

Table 3. Equilibrium distances (R_e, Å) for the ground state (X) and the first excited state (A) of LiH.

Method	Basis Set	X State	A State	Ref.
expt.	not applicable	1.60	2.60	[36]
CMS-PDFT[a]	aug-cc-pVTZ	1.60	2.33	t.w.[b]
MC-PDFT[c]	aug-cc-pVTZ	1.60	2.91	[19]
FCI	6-311G	1.63	n.a.[d]	[41]

[a]tPBE.
[b]this work.
[c]tPBE.
[d]not available.

The active space for our calculations on HCHO was determined using the previously developed ABC2 automatic active-space selection scheme [42]. We set the parameters A, B, and C of this scheme equal to 3, 2, and 0, respectively. This yields an active space of 6 electrons in 5 orbitals for a state-averaged calculation averaging over two states.

We calculated the equilibrium geometry for the ground state and the first excited singlet state ($n \rightarrow \pi^*$) of HCHO. We optimised the geometries of the ground and first excited singlet state until the root-mean-square (RMS) of the gradient components (i.e. the magnitude of the gradient) is less than 0.0003 hartree/bohr for the ground state and less than 0.001 hartree/bohr for the excited state.

The CMS-PDFT optimised geometric data are shown in Tables 4 and 5, where they are compared to MC-PDFT results based on the same SA-CASSCF reference function and to some other results from previous calculations. Some details of these calculations are given in Table 6. The previous calculations to which we compare include multireference methods and single-reference methods. The multireference comparisons include results [19] from the MC-PDFT calculations with a (12, 12) active space that includes all the valence orbitals and two second-shell oxygen long pair orbitals and results [43] from CASPT2 calculations with a (12, 10) active space that includes all valence orbitals. The comparisons also include results from some high-level single-reference methods, including results [43] from the third-order coupled cluster (CC3) [44,45] method, results [43] from the second-order algebraic diagrammatic construction (ADC(2)) [46], method, and results [43] from the the coupled cluster response method with single and double excitations and noniterative connected triple excitations from CC3 (CCSDR(3)) [47]. These three methods have been previously shown to perform well for excitation energies [43,48–52].

Tables 4 and 5 also contains the experimental values. The experimental data for the ground state geometry come from the reinterpreted results [53] of the millimetre

Table 4. Bond lengths (Å) and bond angles (degree) obtained with various methods for the ground state of HCHO.

Method	Ref.	r(CO)	r(CH)	θ(HCH)
CMS-PDFT(6, 5)	t.w.[a]	1.203	1.112	115.8
MC-PDFT(6, 5)	t.w.	1.202	1.112	115.8
MC-PDFT(12, 12)	[19]	1.210	1.114	116.1
CASPT2(12, 10)	[43]	1.209	1.102	116.1
ADC(2)	[43]	1.209	1.096	116.5
CCSDR(3)	[43]	1.207	1.099	116.5
CC3	[43]	1.208	1.100	116.4
expt.	[53]	1.203	1.100	116.2

[a]This work.

Table 5. Bond lengths, H–C–H bond angles, θ, and the C = O out-of-plane angle, η, obtained with various methods for the first excited state of HCHO. Bond lengths are in Å and angles are in degrees.

Method	Ref.	r(CO)	r(CH)	θ(HCH)	η
CMS-PDFT(6, 5)	t.w.[a]	1.333	1.095	119.9	30
MC-PDFT(6, 5)	t.w.	1.333	1.095	119.9	30
MC-PDFT(12, 12)	[19]	1.323	1.102	117.6	28
CASPT2(12, 10)	[43]	1.326	1.090	118.1	38
ADC(2)	[43]	1.380	1.081	123.8	19
CCSDR(3)	[43]	1.320	1.089	118.2	37
CC3	[43]	1.326	1.089	118.3	37
expt.	[55]	1.323	1.098	118.4	34

[a]This work.

Table 6. Computational details of the theoretical calculations in this work and in the literature.

Method	n_{SA}	Active Space	Basis Set	Ref.
CMS-PDFT	2	(6, 5)	jun-cc-pVTZ	t.w.[a]
MC-PDFT	2	(6, 5)	jun-cc-pVTZ	t.w.
MC-PDFT	2	(12, 12)	aug-cc-pVTZ	[19]
CASPT2		(12, 10)	aug-cc-pVTZ	[43]
ADC(2)	n/a[b]	n/a	aug-cc-pVTZ	[52]
CCSDR(3)	n/a	n/a	aug-cc-pVTZ	[52]
CC3	n/a	n/a	aug-cc-pVTZ	[43,52]

[a]This work.
[b]Not applicable.

wave spectrum of formaldehyde [54]. The experimental excited-state geometry comes from the fitting [55] of the HCHO absorption spectra [56,57]. We use the experimental values as reference values.

The CMS-PDFT geometries have similar accuracy to those by the rest of the methods listed in Tables 4 and 5. The CMS-PDFT calculation gives the second most accurate out-of-plane angle, η, among the methods listed. The table shows that CMS-PDFT with the (6, 5) active space gives the same results as MC-PDFT with the (6, 5) active space for the two excitations studied here for HCHO; the reason for this is later discussed in Table 8.

The theoretical adiabatic and vertical excitation energies are shown in Table 7. Previous work for a large set of molecules has shown that the CC3 method usually agrees with extrapolated full configuration interaction (FCI) calculations within 0.03 eV [48], so we use the CC3

Table 7. The first adiabatic and vertical excitation energies (eV) of HCHO.

		$E_{S_1} - E_{S_0}$	
Method	Ref.	Adiabatic	Vertical
CMS-PDFT(6, 5)	t.w.[a]	3.65	4.07
MC-PDFT(6, 5)	t.w.	3.65	4.07
MC-PDFT(12, 12)	[19]	3.58	3.92
CASPT2(12, 10)	[43]	3.53	3.92
ADC(2)	[43]		3.92
CCSDR(3)	[43]		3.97
CC3	[43,52]	3.58	3.96

[a]This work.

Table 8. Rotation matrix in Equation (4) for generating the CMS intermediate states for the ground-state (GS) and the first excited singlet state (ES) equilibrium geometries.

SA-CASSCF	Intermediate State	
States	$\|S_0\rangle$	$\|S_1\rangle$
	GS equilibrium	
S_0	1.0	-3.5×10^{-11}
S_1	3.5×10^{-11}	1.0
	ES equilibrium	
S_0	1.0	-1.1×10^{-9}
S_1	1.1×10^{-9}	1.0

results as our reference for excitation energies. Comparing the present results with the CC3 results, we see that both the adiabatic and the vertical excitation energy are overestimated by CMS-PDFT and MC-PDFT calculations with the (6, 5) active space, but by less than 0.1 eV. The MC-PDFT calculation with the larger active space, (12, 12), is more accurate than the CMS-PDFT or MC-PDFT calculations with the smaller active space. The CASPT2 calculation with the (12, 10) active space is also more accurate than the smaller-active-space calculations.

Table 8 shows the rotation matrix elements $\langle I|P\rangle$ of Equation (4) that are used for calculating HCHO CMS intermediate states from the SA-CASSCF states. We see that the ground state and the first excited state are hardly mixed in the CMS intermediate states for the two states under consideration here at either the ground-state or the first-excited state equilibrium geometry. This explains why the CMS-PDFT results and the MC-PDFT results with the (6, 5) active space are identical for geometries and excitation energies in this case. The case considered next (phenol) involves significant mixing of the SA-CASSCF states in the intermediate states, and in that case the MC-PDFT and CMS-PDFT geometries and excitation energies will differ.

4.3. Phenol

The 11 active orbitals of the phenol molecule are three π orbitals, three π^* orbitals, one oxygen $2p_z$ orbital, and one pair each of C–O and O–H σ and σ^* orbitals.

Table 9. Vertical and adiabatic S_0–S_1 excitation energies of phenol in eV, not including vibrational ZPE, computed with various methods and compared to excitation energies reported in the literature.

	n_{SA}	Active space	Basis set	Ref.	$E_{S_1} - E_{S_0}$ Vertical	Adiabatic
SA-CASSCF	3	(12, 11)	2ζ	t.w.[a]	4.929	4.729
MC-PDFT	3	(12, 11)	2ζ	t.w.	5.025	4.829
CMS-PDFT	3	(12, 11)	2ζ	t.w.	4.929	4.720
CASPT2//CASSCF	1	(8, 8)	2ζ	[58]	4.643	4.364
CASPT2//CASSCF	4	(10,10)	3ζ	[59]	4.52	4.37
CC2//MP2[b]	1	n/a[c]	2ζ	[60]	4.864	4.673
MRCI//CASSCF		(10, 9)	2ζ	[61]	4.75[d]	4.816
MRCI PES fit	9	(12, 14)[e]	2ζ	[62]		4.885
Semiemp. PES fit	9	(12, 14)[e]	2ζ	[63]	4.829	4.661

Note: A model space size of 1 corresponds to state-specific calculations. See text concerning experimental interpretations.
[a]This work.
[b]Geometry optimisation of S_1 carried out at CC2 level.
[c]Not applicable.
[d]Vertical excitation energies can appear lower than adiabatic ones when excitation energies are calculated at geometries optimised with a different level of theory.
[e]Restricted active space consisting only of single and double excitations from a reference determinant.

Table 9 compares our computed vertical and adiabatic excitation energies at the SA-CASSCF, MC-PDFT, and CMS-PDFT levels to results of similar calculations carried out at other levels of theory reported in the literature. Note that vibrational zero-point energy (ZPE) is not included, meaning that direct experimental comparison is not possible. However, Ref. [63] reports a potential energy surface fit which is parameterised to replicate the ZPE-inclusive experimental adiabatic excitation energy of 4.507 eV [64,65], and the ZPE contribution to the adiabatic excitation energy predicted by this surface agrees with that reported by Refs. [61,62] to within 0.01 eV. Therefore, taking the results of Ref. [63] (reported in the last row of Table 9) as a reference, we evaluate the error of our SA-CASSCF, MC-PDFT with an SA-CASSCF wave function, and CMS-PDFT adiabatic excitation energies as being about +0.07, +0.17, and +0.06 eV, respectively. We also note that, other than Ref. [61], all of the calculations reported in Table 9 describe a vertical excitation energy roughly 0.2 eV higher than the adiabatic one.

Table 11 presents a selection of optimised internal coordinates corresponding to some of the the adiabatic excitation energies reported in Table 9. In general, we observe that CMS-PDFT geometries resemble SA-CASSCF geometries more than MC-PDFT geometries. Most bond lengths in all calculations agree with experimental bond lengths in both states to within 0.01 Å, and the C–O–H bond angles agree with experiment to within 1 degree. However, uniquely, the MC-PDFT optimised geometry of phenol in the S_1 state is nonplanar, with a significant nonzero C–C–O–H dihedral angle.

Table 10. Relative MC-PDFT and CMS-PDFT energies of phenol in eV at the CMS-PDFT S_1 optimised geometry ('flat') and the MC-PDFT S_1 optimised geometry ('bent'), along with unitary columns describing the optimised CMS-PDFT intermediate states in terms of reference states at those geometries.

	Energy		Intermediate state vectors		
	MC-PDFT	CMS-PDFT	$\|S_0\rangle$	$\|S_1\rangle$	$\|S_2\rangle$
			Flat geometry		
S_0	0.00[a]	0.14	0.713	0.701	0.000
S_1	4.66	4.65	0.701	−0.713	0.000
S_2	5.88	5.88	0.000	0.000	1.000
			Bent geometry		
S_0	0.09	0.22	−0.708	−0.706	−0.019
S_1	4.64	4.70	0.691	−0.688	−0.223
S_2	5.82	5.91	0.144	−0.171	0.975

Note: Note that every row and column of the unitary matrix carries an arbitrary sign.
[a]The MC-PDFT S_0 total energy of −307.049728 E_h at the flat geometry is taken as the reference.

Table 11. Selected internal coordinates of phenol in the S_0 and S_1 states computed by various methods as well as experiment. Bond lengths are in Å and angles are in degrees.

State	Method	Ref.	Avg. r_{CC}	r_{CO}	r_{OH}	θ_{COH}	ϕ_{CCOH}
S_0	SA-CASSCF	t.w.[a]	1.399	1.384	0.966	109.3	0
	MC-PDFT	t.w.	1.401	1.37	0.964	109.2	0
	CMS-PDFT	t.w.	1.398	1.367	0.966	109.2	0
	MRCI PES fit	[62]	1.395	1.382	0.964	108.6	0
	Expt.	[66]	1.393	1.375	0.957	108.8	0
S_1	CASSCF	t.w.	1.434	1.379	0.96	109.3	0
	MC-PDFT	t.w.	1.429	1.337	0.975	108.2	14.3
	CMS-PDFT	t.w.	1.435	1.362	0.962	109.2	0
	MRCI PES fit	[62]	1.427	1.367	0.963	108.7	0
	Expt.	[67]	1.423	1.356	0.992	108.8	0

[a]This work.

This nonphysical result corresponds to the greater estimated error of the adiabatic excitation energies discussed above.

CMS-PDFT correctly predicts a flat, planar optimised S_1 geometry of phenol, unlike MC-PDFT. The mechanism for this correction, and the reason for the underlying failure of MC-PDFT, is probed in Table 10. Somewhat surprisingly, although all methods agree that S_1 and S_2 are much closer in energy to each other than to S_0, Table 10 shows that in the intermediate basis of the model space, the interaction between the S_1 and S_0 states, rather than that between S_1 and S_2, is the main relevant state-interaction effect. At both geometries, the lowest two optimised CMS-PDFT intermediate states in terms of the SA-CASSCF reference states are approximately $2^{-1/2}(|S_0\rangle \pm |S_1\rangle)$. Although the 'bent' optimised MC-PDFT S_1 geometry has an energy that is 0.02 eV lower than that of the 'flat' geometry, the S_0 MC-PDFT energy at the bent geometry is 0.09 eV higher. The nearly 50–50 mixture of the two reference states means that the destabilisation of S_0 'wins out' over the stabilisation of

S_1, and the CMS-PDFT S_1 energy at the bent geometry is 0.05 eV higher than at the flat geometry.

5. Conclusion

In this paper, we report the implementation of the CMS-PDFT analytic gradient in both *OpenMolcas* and *PySCF*, and we present the Lagrange multiplier equations that are used for the implementation. We compare the results of two programmes for HeH^+ and the results show that two implementations agree with each other very well. We also compared the analytic gradient with the numerical gradient for three diatomic systems, HeH^+, LiH, and LiF, to show that the analytic gradient is accurate. We also showed that we are able to optimise excited-state geometries of formaldehyde and phenol with the implemented analytic gradients, and the results show that CMS-PDFT produces reasonable geometries for ground and excited states and reasonable adiabatic excitation energies using these optimised geometries. We find that CMS-PDFT is more accurate than MC-PDFT for the excited-state geometry of phenol. Our results indicate that CMS-PDFT is a promising method for studying excited states with strong state interaction.

Acknowledgments

The authors are grateful to David Yarkony and Christopher Malbon for providing the vertical excitation energy of the S_1 state of phenol from their potential energy surface of Ref. [63]. Any opinions, findings, and conclusions or recommendations expressed in this material are those of the author(s) and do not necessarily reflect the views of the National Science Foundation.

Disclosure statement

No potential conflict of interest was reported by the author(s).

Funding

The present work is supported by the National Science Foundation under grant CHE-2054723. R.L. acknowledges the Swedish Research Council (VR, Grant 2020-03182) for funding. T.R.S. acknowledges that this material is also based upon work supported by the National Science Foundation Graduate Research Fellowship Program under Grant No. DGE 1746045, Project No. 00074041.

ORCID

Jie J. Bao http://orcid.org/0000-0003-0197-3405
Matthew R. Hermes http://orcid.org/0000-0001-7807-2950
Thais R. Scott http://orcid.org/0000-0002-5746-5517
Andrew M. Sand http://orcid.org/0000-0002-7166-2066
Roland Lindh http://orcid.org/0000-0001-7567-8295
Laura Gagliardi http://orcid.org/0000-0001-5227-1396
Donald G. Truhlar http://orcid.org/0000-0002-7742-7294

References

[1] W.G. Dauben, L. Salem and N.J. Turro, Acc. Chem. Res. **8**, 41 (1975). doi:10.1021/cen-v046n004.p005.
[2] P.E. Siegbahn, J. Chem. Phys. **70**, 5391 (1979). doi:10.1063/1.437473.
[3] P.E. Siegbahn, J. Chem. Phys. **72**, 1647 (1980). doi:10.1063/1.439365.
[4] A.A. Granovsky, J. Chem. Phys. **134**, 214113 (2011). doi:10.1063/1.3596699.
[5] C. Angeli, S. Borini, M. Cestari and R. Cimiraglia, J. Chem. Phys. **121**, 4043 (2004). doi:10.1063/1.1778711.
[6] T. Shiozaki, W. Győrffy, P. Celani and H.-J. Werner, J. Chem. Phys. **135**, 081106 (2011). doi:10.1063/1.3633329.
[7] S. Battaglia and R. Lindh, J. Chem. Theory Comput. **16**, 1555 (2020). doi:10.1021/acs.jctc.9b01129.
[8] S. Battaglia and R. Lindh, J. Chem. Phys. **154**, 034102 (2021). doi:10.1063/5.0030944.
[9] G.L. Manni, R.K. Carlson, S. Luo, D. Ma, J. Olsen, D.G. Truhlar and L. Gagliardi, J. Chem. Theory Comput. **10**, 3669 (2014). doi:10.1021/ct500483t.
[10] L. Gagliardi, D.G. Truhlar, G. Li Manni, R.K. Carlson, C.E. Hoyer and J.L. Bao, Acc. Chem. Res.**50**, 66 (2017). doi:10.1021/acs.accounts.6b00471.
[11] P. Sharma, J.J. Bao, D.G. Truhlar and L. Gagliardi, Annu. Rev. Phys. Chem. **72**, 541 (2021). doi:10.1146/physchem.2021.72.issue-1.
[12] A.M. Sand, C.E. Hoyer, D.G. Truhlar and L. Gagliardi, J. Chem. Phys. **149**, 24106 (2018). doi:10.1063/1.5036727.
[13] J.J. Bao, C. Zhou, Z. Varga, S. Kanchanakungwankul, L. Gagliardi and D.G. Truhlar, Faraday Discuss.**224**, 348 (2020). doi:10.1039/d0fd00037j.
[14] J.J. Bao, C. Zhou and D.G. Truhlar, J. Chem. Theory. Comput. **16**, 7444 (2020). doi:10.1021/acs.jctc.0c00908.
[15] T. Helgaker and P. Jørgensen, Theor. Chim. Acta **75**, 111 (1989). doi:10.1007/BF00527713.
[16] P. Jørgensen and T. Helgaker, J. Chem. Phys. **89**, 1560 (1988). doi:10.1063/1.455152.
[17] J. Stålring, A. Bernhardsson and R. Lindh, Mol. Phys. **99**, 103 (2001). doi:10.1080/002689700110005642.
[18] A.M. Sand, C.E. Hoyer, K. Sharkas, K.M. Kidder, R. Lindh, D.G. Truhlar and L. Gagliardi, J. Chem. Theory Comput. **14**, 126 (2018). doi:10.1021/acs.jctc.7b00967.
[19] T.R. Scott, M.R. Hermes, A.M. Sand, M.S. Oakley, D.G. Truhlar and L. Gagliardi, J. Chem. Phys.**153**, 014106 (2020). doi:10.1063/5.0007040.
[20] T.R. Scott, M.S. Oakley, M.R. Hermes, A.M. Sand, M.S. Oakley, R. Lindh, D.G. Truhlar and L. Gagliardi, J. Chem. Phys. **154**, 074108 (2021). doi:10.1063/5.0007040.
[21] I. Fdez. Galván, M. Vacher, A. Alavi, C. Angeli, F. Aquilante, J. Autschbach, J.J. Bao, S.I. Bokarev, N.A. Bogdanov, R.K. Carlson, L.F. Chibotaru, J. Creutzberg, N. Dattani, M.G. Delcey, S.S. Dong, A. Dreuw, L. Freitag, L.M. Frutos, L. Gagliardi, F. Gendron, A. Giussani, L. González, G. Grell, M. Guo, C.E. Hoyer, M. Johansson, S. Keller, S. Knecht, G. Kovačević, E. Källman, G. Li Manni, M. Lundberg, Y. Ma, S. Mai, J.P. Malhado, P.Å. Malmqvist, P. Marquetand, S.A. Mewes, J. Norell, M. Olivucci, M. Oppel, Q.M. Phung, K. Pierloot, F. Plasser, M. Reiher, A.M. Sand, I. Schapiro, P. Sharma, C.J. Stein, L.K. Sørensen, D.G. Truhlar, M. Ugandi, L.

Ungur, A. Valentini, S. Vancoillie, V. Veryazov, O. Weser, T.A. Wesołowski, P.O. Widmark, S. Wouters, A. Zech, J.P. Zobel and R. Lindh, J. Chem. Theory Comput. **15**, 5925 (2019). doi:10.1021/acs.jctc.9b00532.

[22] F. Aquilante, J. Autschbach, A. Baiardi, S. Battaglia, V.A. Borin, L.F. Chibotaru, I. Conti, L. De Vico, M. Delcey, I.F. Galván, N. Ferré, L. Freitag, M. Garavelli, X. Gong, S. Knecht, E.D. Larsson, R. Lindh, M. Lundberg, P.Å. Malmqvist, A. Nenov, J. Norell, M. Odelius, M. Olivucci, T.B. Pedersen, L. Pedraza-González, Q.M. Phung, K. Pierloot, M. Reiher, I. Schapiro, J. Segarra-Martí, F. Segatta, L. Seijo, S. Sen, D.-C. Sergentu, C.J. Stein, L. Ungur, M. Vacher, A. Valentini and V. Veryazov, J. Chem. Phys. **152**, 214117 (2020). doi:10.1063/5.0004835.

[23] M.R. Hermes, ⟨https://github.com/MatthewRHermes/mrh⟩ (2018).

[24] Q. Sun, X. Zhang, S. Banerjee, P. Bao, M. Barbry, N.S. Blunt, N.A. Bogdanov, G.H. Booth, J. Chen, Z.-H. Cui, J.J. Eriksen, Y. Gao, S. Guo, J. Hermann, M.R. Hermes, K. Koh, P. Koval, S. Lehtola, Z. Li, J. Liu, N. Mardirossian, J.D. McClain, M. Motta, B. Mussard, H.Q. Pham, A. Pulkin, W. Purwanto, P.J. Robinson, E. Ronca, E. Sayfutyarova, M. Scheurer, H.F. Schurkus, J.E.T. Smith, C. Sun, S.-N. Sun, S. Upadhyay, L.K. Wagner, X. Wang, A. White, J.D. Whitfield, M.J. Williamson, S. Wouters, J. Yang, J.M. Yu, T. Zhu, T.C. Berkelbach, S. Sharma, A.Y. Sokolov and G.K.-L. Chan, J. Chem. Phys. **153**, 024109 (2020). doi:10.1063/5.0006074.

[25] L.-P. Wang and C. Song, J. Chem. Phys. **144**, 214108 (2016). doi:10.1063/1.4952956.

[26] T.H. Dunning Jr., J. Chem. Phys. **90**, 1007 (1989). doi:10.1063/1.456153.

[27] E. Papajak, J. Zheng, X. Xu, H.R. Leverentz and D.G. Truhlar, J. Chem. Theory Comput. **7**, 3027 (2011). doi:10.1021/ct200106a.

[28] G. Glockler and D. Fuller, J. Chem. Phys. **1**, 886 (1933). doi:10.1063/1.1749262.

[29] D.M. Bishop and L.M. Cheung, J. Mol. Spectrosc. **75**, 462 (1979). doi:10.1016/0022-2852(79)90090-0.

[30] S. Peyerimhoff, J. Chem. Phys. **43**, 998 (1965). doi:10.1063/1.1696884.

[31] R. Güsten, H. Wiesemeyer, D. Neufeld, K.M. Menten, U.U. Graf, K. Jacobs, B. Klein, O. Ricken, C. Risacher and J. Stutzki, Nature **568**, 357 (2019). doi:10.1038/s41586-019-1090-x.

[32] O. Novotný, P. Wilhelm, D. Paul, Á. Kálosi, S. Saurabh, A. Becker, K. Blaum, S. George, J. Göck, M. Grieser, F. Grussie, R. von Hahn, C. Krantz, H. Kreckel, C. Meyer, P.M. Mishra, D. Muell, F. Nuesslein, D.A. Orlov, M. Rimmler, V.C. Schmidt, A. Shornikov, A.S. Terekhov, S. Vogel, D. Zajfman and A. Wolf, Science **365**, 676 (2019). doi:10.1126/science.aax5921.

[33] R.J. Fallon, J.T. Vanderslice and E.A. Mason, J. Chem. Phys. **32**, 1453 (1960). doi:10.1063/1.1730940.

[34] K.C. Li and W.C. Stwalley, J. Mol. Spectrosc. **69**, 294 (1978). doi:10.1016/0022-2852(78)90066-8.

[35] A. Pardo, J.J. Camacho and J.M.L. Poyato, Chem. Phys. Lett. **131**, 490 (1986). doi:10.1016/0009-2614(86)80570-X.

[36] W.C. Stwalley and W.T. Zemke, J. Phys. Chem. Ref. Data **22**, 87 (1993). doi:10.1063/1.555936.

[37] W.-C. Tung, M. Pavanello and L. Adamowicz, J. Chem. Phys. **134**, 64117 (2011). doi:10.1063/1.3554211.

[38] A.D. Bandrauk and J.M. Gauthier, J. Phys. Chem. **93**, 7552 (1989). doi:10.1021/j100359a007.

[39] A. McLean, J. Chem. Phys. **39**, 2653 (1963). doi:10.1063/1.1734078.

[40] G. Benson and B. Van der Hoff, J. Chem. Phys. **22**, 469 (1954). doi:10.1063/1.1740092.

[41] A.M. Maniero and P.H. Acioli, Int. J. Quantum Chem. **103**, 711 (2005). doi:10.1002/(ISSN)1097-461X.

[42] J.J. Bao and D.G. Truhlar, J. Chem. Theory Comput. **15**, 5308 (2019). doi:10.1021/acs.jctc.9b00535.

[43] Š. Budzák, G. Scalmani and D. Jacquemin, J. Chem. Theory Comput. **13**, 6237 (2017). doi:10.1021/acs.jctc.7b00921.

[44] O. Christiansen, H. Koch and P. Jörgensen, J. Chem. Phys. **103**, 7429 (1995). doi:10.1063/1.470315.

[45] H. Koch, O. Christiansen, P. Jörgensen, A.M. Sanchez de Merás and T. Helgaker, J. Chem. Phys. **106**, 1808 (1997). doi:10.1063/1.473322.

[46] A. Dreuw and M. Wormit, WIREs Comput. Mol. Sci. **5**, 82 (2015). doi:10.1002/wcms.1206.

[47] O. Christiansen, H. Koch and P. Jörgensen, J. Chem. Phys. **105**, 1451 (1996). doi:10.1063/1.472007.

[48] P.-F. Loos, A. Scemama, A. Blondel, Y. Garniron, M. Caffarel and D. Jacquemin, J. Chem. Theory Comput. **14**, 4360 (2018). doi:10.1021/acs.jctc.8b00406.

[49] P.-F. Loos, F. Lipparini, M. Boggio-Pasqua, A. Scemama and D. Jacquemin, J. Chem. Theory Comput.**16**, 1711 (2020). doi:10.1021/acs.jctc.9b01216.

[50] P.-F. Loos, A. Scemama, M. Boggio-Pasqua and D. Jacquemin, J. Chem. Theory Comput. **16**, 3720 (2020). doi:10.1021/acs.jctc.0c00227.

[51] P.-F. Loos and D. Jacquemin, J. Phys. Chem. A **125**, 10174 (2021). doi:10.1021/acs.jpca.1c08524.

[52] D. Jacquemin, J. Chem. Theory Comput. **14**, 1534 (2018). doi:10.1021/acs.jctc.7b01224.

[53] J.L. Duncan, Mol. Phys. **28**, 1177 (1974). doi:10.1080/00268977400102501.

[54] K. Takagi and T. Oka, J. Phys. Soc. Jpn. **18**, 1174 (1963). doi:10.1143/JPSJ.18.1174.

[55] P. Jensen and P.R. Bunker, J. Mol. Spectrosc. **94**, 114 (1982). doi:10.1016/0022-2852(82)90298-3.

[56] F. Birss, R. Gordon, D. Ramsay and S. Till, Can. J. Phys. **57**, 1676 (1979). doi:10.1139/p79-232.

[57] V. Job, V. Sethuraman and K. Innes, J. Mol. Spectrosc. **30**, 365 (1969). doi:10.1016/0022-2852(69)90274-4.

[58] G. Granucci, J.T. Hynes, P. Millié and T.-H. Tran-Thi, J. Am. Chem. Soc. **122**, 12243 (2000). doi:10.1021/ja993730j.

[59] R.N. Dixon, T.A. Oliver and M.N. Ashfold, J. Chem. Phys. **134**, 194303 (2011). doi:10.1063/1.3585609.

[60] G.A. Pino, A.N. Oldani, E. Marceca, M. Fujii, S.-I. Ishiuchi, M. Miyazaki, M. Broquier, C. Dedonder and C. Jouvet, J. Chem. Phys. **133**, 124313 (2010). doi:10.1063/1.3480396.

[61] O.P. Vieuxmaire, Z. Lan, A.L. Sobolewski and W. Domcke, J. Chem. Phys. **129**, 224307 (2008). doi:10.1063/1.3028049.

[62] X. Zhu and D.R. Yarkony, J. Chem. Phys. **144**, 024105 (2016). doi:10.1063/1.4938236.
[63] X. Zhu, C.L. Malbon and D.R. Yarkony, J. Chem. Phys. **144**, 124312 (2016). doi:10.1063/1.4944091.
[64] W. Roth, P. Imhof, M. Gerhards, S. Schumm and K. Kleinermanns, Chem. Phys. **252**, 247 (2000). doi:10.1016/S0301-0104(99)00326-2.
[65] M.L. Hause, Y.H. Yoon, A.S. Case and F.F. Crim, J. Chem. Phys. **128**, 104307 (2008). doi:10.1063/1.2831512.
[66] N.W. Larsen, J. Mol. Struct. **51**, 175 (1979). doi:10.1016/0022-2860(79)80292-6.
[67] D. Spangenberg, P. Imhof and K. Kleinermanns, Phys. Chem. Chem. Phys. **5**, 2505 (2003). doi:10.1039/b301228j.